Mechanism underlying selective regulation of G protein-gated inwardly rectifying potassium channels by the psychostimulant-sensitive sorting nexin 27

Bartosz Balana[a], Innokentiy Maslennikov[b], Witek Kwiatkowski[b], Kalyn M. Stern[a], Laia Bahima[a], Senyon Choe[b,1], and Paul A. Slesinger[a,1]

[a]Clayton Foundation Laboratories for Peptide Biology and [b]Structural Biology Laboratory, Salk Institute for Biological Studies, La Jolla, CA 92037

Edited by David E. Clapham, Children's Hospital Boston, Howard Hughes Medical Institute, Boston, MA, and approved February 25, 2011 (received for review December 15, 2010)

G protein-gated inwardly rectifying potassium (GIRK) channels are important gatekeepers of neuronal excitability. The surface expression of neuronal GIRK channels is regulated by the psychostimulant-sensitive sorting nexin 27 (SNX27) protein through a class I (-X-Ser/Thr-X-Φ, where X is any residue and Φ is a hydrophobic amino acid) PDZ-binding interaction. The G protein-insensitive inward rectifier channel (IRK1) contains the same class I PDZ-binding motif but associates with a different synaptic PDZ protein, postsynaptic density protein 95 (PSD95). The mechanism by which SNX27 and PSD95 discriminate these channels was previously unclear. Using high-resolution structures coupled with biochemical and functional analyses, we identified key amino acids upstream of the channel's canonical PDZ-binding motif that associate electrostatically with a unique structural pocket in the SNX27-PDZ domain. Changing specific charged residues in the channel's carboxyl terminus or in the PDZ domain converts the selective association and functional regulation by SNX27. Elucidation of this unique interaction site between ion channels and PDZ-containing proteins could provide a therapeutic target for treating brain diseases.

Kir3 | Kir2 | endosome | inhibition

G protein-gated inwardly rectifying potassium (GIRK, or Kir3) channels are important regulators of neuronal excitability and have been implicated in various excitability disorders including epilepsy, Down syndrome, Parkinson's disease, and drug addiction (1). Activation of GIRK channels reduces membrane excitability, resulting in inhibition of the neuron-firing rate. As part of a larger macromolecular signaling complex, GIRK channels are activated directly by G protein Gβγ subunits (2, 3) following stimulation of G protein-coupled receptors (GPCRs), such as $GABA_B$ and M_2 muscarinic receptors (1). Three primary GIRK subunits—GIRK1, GIRK2 (including 2a, 2b, and 2c splice variants), and GIRK3—coexist in the brain and assemble into heterotetramers (e.g., GIRK1/2, GIRK1/3, GIRK2/3) or homotetramers (GIRK2 only). Recent studies have started to demonstrate that GIRK channel signaling is dynamically regulated in neurons, changing in response to neuronal activity and stimulation of GPCRs (4–7).

Movement of GIRK channels within cells is controlled by various intrinsic amino acid sequence motifs that control ER export, internalization from plasma membranes, lysosomal targeting, and association with trafficking proteins (8, 9). Recently, we found that surface expression of GIRK3-containing channels is reduced by association with sorting nexin 27 (SNX27) (6). SNX27 is a member of a large family of endosomal trafficking protein (10) and has two splice forms (SNX27a and SNX27b) that vary only in the C-terminal end. SNX27 protein has been detected in synaptosomes purified from mouse cortex (11), but its expression in the brain has not been well characterized. In addition to GIRK channels, SNX27 associates with some GPCRs, including the 5-HT4a serotonin receptor (12) and the β2 adrenergic receptor (13), as well as with a kinase (14). Interestingly, the *Snx27b* splice variant transcript (also known as methamphetamine-responsive transcript 1) is upregulated in rodents addicted to psychostimulants, such as cocaine and methamphetamine (15, 16). Thus, SNX27 is emerging as a potential link between drugs of abuse and the trafficking of 5-HT4a receptors and GIRK channels.

Both GIRK2c and GIRK3 contain a class I PDZ (PSD95/disc large/zona occludens)- binding motif that associates directly with the PDZ domain of SNX27a/b. If the last four amino acids match the consensus sequence of -X-Ser/Thr-X-Φ or -X-Φ-X-Φ (where X is any residue and Φ is a hydrophobic amino acid), then the protein is broadly categorized as class I or II, respectively (17, 18). However, the presence of a particular PDZ-binding motif does not always predict the appropriate binding partner; for example, the C-terminal motif of GIRK2c/3 channels ends in -ESKV and associates directly with the SNX27-PDZ domain, but not with the PDZ domain of the postsynaptic density protein 95 (PSD95) (6). Conversely, the localization of voltage-gated K channels (Kv1.4-ETDV) and G protein-insensitive IRK1 (Kir2.1-ESEI) channels (19) is controlled by the PDZ domain of PSD95, but not by SNX27 (6, 20, 21; but see ref. 22). The mechanism underlying this type of class I PDZ selectivity is incompletely understood. Neurons contain a wide range of PDZ domain-containing proteins that must choose their appropriate target proteins (19). Determining the structural mechanism underlying the specificity of binding among class I PDZ-containing proteins is essential for understanding the complexity of PDZ interactions that are important for regulating neuronal excitability. In the present study, we combined structural, biochemical, and functional approaches to reveal the mechanism underlying the regulation of GIRK3 and IRK1 by SNX27 and PSD95, respectively.

Results

Snx27b mRNA is expressed in diverse brain regions, including the hippocampus, cortex, and cerebellum (6). We generated a rabbit antibody specific for the N-terminal domain of SNX27a/b (*Materials and Methods* and Fig. S1) and performed double-immunofluorescence staining in rat hippocampus sections for SNX27a/b and neuronal nuclei marker NeuN, microtubule-associated protein-2 (MAP2) to label dendritic fields, or glial fibrillar-associated protein (GFAP). SNX27a/b was present mostly in dendritic fields and perisomatic regions of pyramidal neurons in CA1 hippocampus,

Author contributions: B.B., S.C., and P.A.S. designed research; B.B., I.M., W.K., K.M.S., and L.B. performed research; L.B. contributed new reagents/analytical tools; B.B., I.M., W.K., S.C., and P.A.S. analyzed data; and B.B. and P.A.S. wrote the paper.

The authors declare no conflict of interest.

This article is a PNAS Direct Submission.

Database deposition: The atomic coordinates and structure factors have been deposited in the Protein Data Bank, www.pdb.org (PDB ID codes 3QE1, 3QDO, and 3QGL).

[1]To whom correspondence may be addressed. E-mail: slesinger@salk.edu or choe@salk.edu.

This article contains supporting information online at www.pnas.org/lookup/suppl/doi:10.1073/pnas.1018645108/-/DCSupplemental.

as well as in glial cells (Fig. 1*A*). The subcellular localization of endogenous SNX27a/b was analyzed by immunostaining cultured rat hippocampal neurons. SNX27a/b was found to be expressed in puncta distributed thorough the neuron soma and dendrites and colocalized with early endosome antigen 1 (Fig. 1*C*), similar to the findings of previous studies (6, 12, 13).

The expression of SNX27 in early endosomes (Fig. 1*C*) and colocalization with GIRK channels (6) suggest that SNX27a/b might regulate natively expressed GIRK currents (Fig. 1*B*). To address this, we focused on the physiology of the psychostimulant-sensitive SNX27b splice and infected cultured hippocampal neurons with a lentivirus encoding SNX27b (tagged with YFP). At 7 d later, SNX27b-YFP protein was visible in the soma and dendrites (Fig. 1*D*). Using whole-cell patch-clamp electrophysiology, we found that baclofen (100 μM) elicited large $GABA_B$ receptor-activated currents (Fig. 1*E*) that were significantly smaller in neurons expressing SNX27b-YFP (Fig. 1 *E* and *F* and Table S1). Similarly, SNX27b-YFP significantly reduced the amplitude of basal Ba^{2+}-sensitive K^+ currents (Fig. 1 *E* and *G*). This indicates that SNX27b can down-regulate $GABA_B$-GIRK signaling in hippocampal neurons, similar to decreases in currents and surface expression observed in heterologous cells (6).

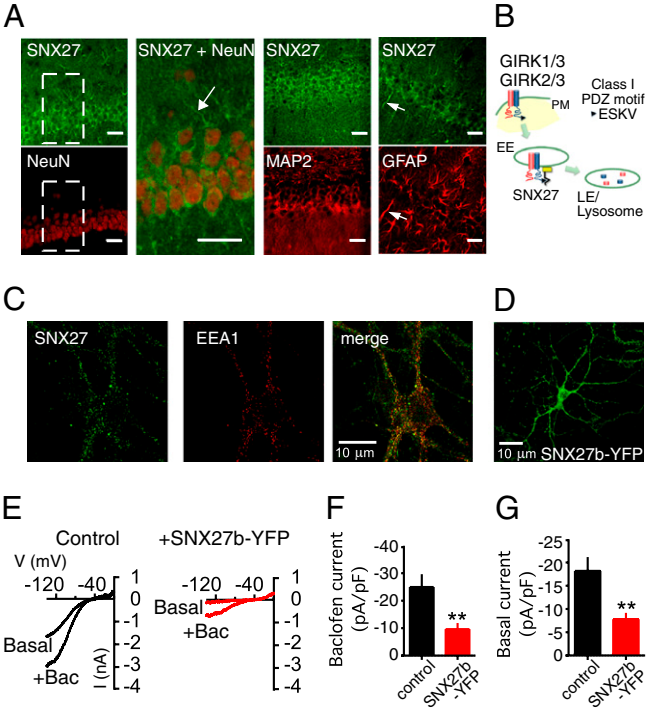

Fig. 1. Expression of SNX27 and regulation of GIRK channels in rat hippocampal neurons. (*A*) Coronal sections of rat CA1 hippocampus immunostained with a pan SNX27 (SNX27a/b; green) antibody and NeuN, MAP2, or GFAP antibody (red). The short arrow highlights glial cells expressing SNX27a/b. (*Inset*) Zoom of CA1 pyramidal neurons for SNX27/NeuN staining; long arrow indicates a dendrite. (Scale bar: 30 μm). (*B*) Schematic for regulation of GIRK channels by SNX27 based on previous studies (6, 7). SNX27 reduces plasma membrane (PM) expression of GIRK channels by targeting GIRK3-containing channels via a class I PDZ motif (ESKV) in to the early endosomes (EE) and subsequent degradation in late endosomes/lysosomes. (*C*) Fluorescent image of cultured rat hippocampal neuron immunostained with pan SNX27 (green) and early endosomal antigen-1 antibody (red). (*D*) Fluorescent image of cultured rat hippocampal neuron infected with SNX27b-YFP lentivirus. (*E*) Current-voltage plots show inwardly rectifying K^+ currents recorded from a neuron expressing GFP (control) or SNX27b-YFP. $GABA_B$ receptor-activated (Bac; 100 μM) and basal Ba^{2+}-sensitive (1 mM) GIRK currents are shown (K_{out} = 20 mM) (Table S1). (*F* and *G*) Bar charts show mean current density, pA/pF, ± SEM. $^{**}P < 0.01$ by the Student *t* test. n = 10–12.

We next investigated the molecular mechanism underlying the association of SNX27b with GIRK channels, which was previously shown to involve the PDZ domain (6). We confirmed that the carboxyl terminus of GIRK3 (fused to GST), but not that of IRK1 or Kv1.4, binds to the isolated PDZ domain (H_8-tagged) of SNX27 (Fig. 2*A*); SNX27a/b contains the same PDZ domain. Conversely, the PDZ1, PDZ2, or PDZ1,2 dimer of PSD95 binds to IRK1 and Kv1.4, but not to the GIRK3 C-terminal sequence (Fig. 2*B*) (20). Thus, GIRK2c, GIRK3, IRK1, and Kv1.4 all contain a C-terminal class I PDZ-binding motif (-X-Ser/Thr-X-Φ) but bind to different PDZ-containing proteins.

We hypothesized that the PDZ domains of SNX27 and PSD95 discriminate among different ion channels using other unknown rules for binding. We first examined the regions implicated previously in class I PDZ-binding specificity (18) (Fig. 2*C*). The canonical carboxylate-binding loop (known as the GLGF loop) contains a Tyr in SNX27-PDZ instead of the more common Leu (Fig. 2*C*). A Y51L mutation into SNX27-PDZ disrupted binding to both GIRK3 and IRK1 C-terminals (Fig. S2). We identified several other candidate amino acids in the vicinity of the PDZ-binding groove that are not conserved between PSD95-PDZ2 and SNX27-PDZ, but these did not create binding to GST-IRK1 (Fig. S2). Thus, none of the mutations in SNX27-PDZ successfully converted binding selectivity from GIRK3 to IRK1.

We then solved a high-resolution (1.68 Å) crystal structure of the SNX27-PDZ domain fused directly to the carboxyl-terminal ESESKV sequence of GIRK3 (SNX27-PDZ-ESESKV) (Fig. 2*D* and Table S2). The basic structural folds of SNX27-PDZ-ESESKV are similar to previously published PDZ structures, with six β strands (βA–βF) and two α helices (αA and αB) folded into a compact β-strand sandwich (18). The ESESKV ligand is bound between the βB strand and the αB helix, where it forms an antiparallel β sheet with the βB strand similar to the ligand bound to the PDZ3 domain of PSD95 (Fig. 2*E*) (23). Below the canonical PDZ-binding cleft, a structural pocket formed by the βB–βC loop was clearly visible (Fig. 2*D*). We confirmed the 3D structural determination and placement of the C-terminal peptide using two additional constructs (*Materials and Methods* and Fig. S3).

What does the SNX27-PDZ structure reveal about GIRK3 binding? Substituting Ile for Val in the 0 position (V^0) of GIRK3 eliminates binding to SNX27-PDZ (6). In all three structures, the side chain of ligand V^0 is located in a hydrophobic groove formed by V55 and F53 of the βB strand and by I119 of the αB helix. In addition, the C-terminal carboxyl group of V^0 is coordinated by the backbone amides of Y51 and G52 in the carboxylate-binding (i.e., GLGF) loop (Fig. 2*E*). This suggests that I119 might sterically limit larger amino acids in the 0 position, like Ile from occupying the pocket (see below). Similar to other PDZ structures, the −4 to 0 residues of the ligand are bound by numerous backbone-to-backbone hydrogen bonds in an antiparallel orientation to the βB strand. The oxygen from the hydroxyl side chain of Ser (S^{-2}) forms a hydrogen bond with nitrogen of the imidazole ring of H112 in the α2 helix, a hallmark of class I PDZ domains (23). Notably, we discovered that glutamate E^{-5} is positioned in a positively charged cavity formed by three Arginines (R56, R66, and R98) originating from βB, βD, and the βB–βC loop (Fig. 2*F*). Because E^{-5} does not appear to form hydrogen bonds with any other residues, we postulated that the positively charged pocket might attract the negatively charged E^{-5}.

To investigate this hypothesis, we carried out a detailed mutation-based analysis of the PDZ ligand. We first replaced the last two amino acids of IRK1 ($E^{-1}I^0$) with those of GIRK3 ($K^{-1}V^0$) to create IRK1-ESKV (IRK1*). IRK1* did not bind to SNX27-PDZ, but retained binding to PSD95-PDZ1,2, similar to WT IRK1 (Fig. 3*A*), confirming that amino acids in the 0 and −1 positions alone are not sufficient for determining the specificity of PDZ binding. We next investigated the role of amino acids located in the −4 and −5 positions ($R^{-5}R^{-4}$ vs. $E^{-5}S^{-4}$) in IRK1* and GIRK3.

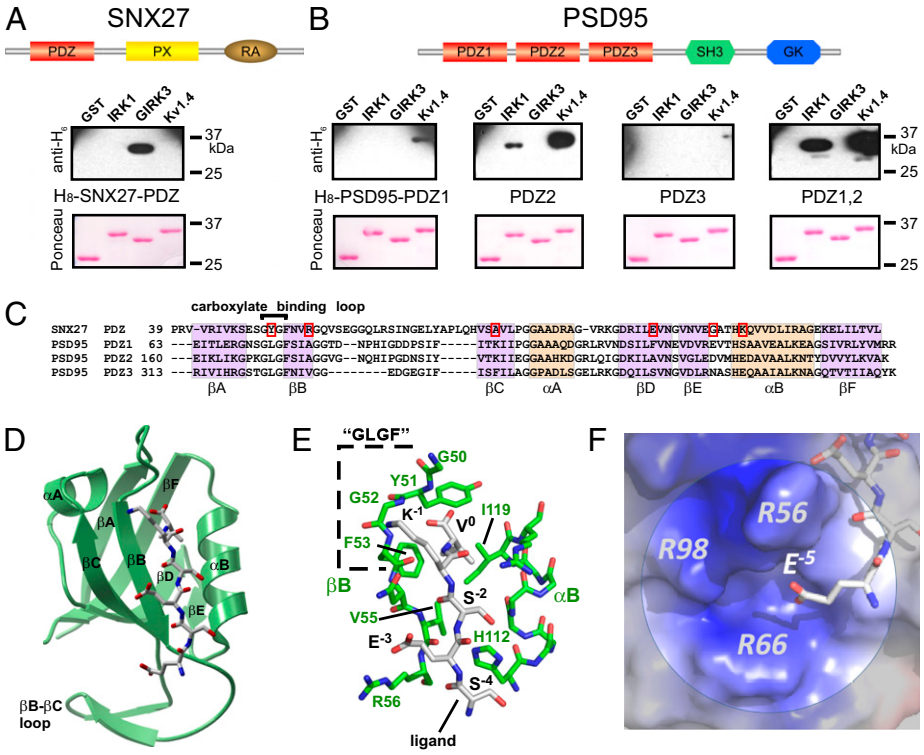

Fig. 2. Structural determination of SNX27-PDZ bound to GIRK3 peptide. (*A* and *B*) Schematics show SNX27 with a lipid-binding Phox domain (PX), a Ras-associating domain (RA), and a single class I PDZ domain (10) and PSD95 with three class I/II PDZ domains, a SH3 domain, and a GK domain (19). (*A*) SNX27-PDZ binds to the GST-tagged carboxyl terminus of GIRK3, but not to that of IRK1 or Kv1.4. (*B*) PSD95-PDZ2 and PSD95-PDZ1,2 bind to IRK1 and Kv1.4, but not to GIRK3. PDZ3 does not bind to IRK1, GIRK3, or Kv1.4. (*Upper*) Immunoblot with anti-H_6 antibody for detecting H_8-tagged probe. (*Lower*) Ponceau S stain for GST proteins. Probes are H_8-SNX27-PDZ (500 nM) or 250 nM H_8-PSD95-PDZ1,2 (250 nM). (*C*) Alignment of PDZ domains for rat SNX27 and PSD95. Red boxes indicate mutations in SNX27-PDZ that did not reverse binding selectivity (Fig. S2). (*D*) High-resolution (1.68 Å) crystal structure of the SNX27-PDZ-ESESKV fusion protein. A ribbon model for the PDZ domain (green) with the bound ESESKV peptide sequence. Residues 0 to −4 of the peptide are tightly bound to the βB strand and αB helix of the PDZ domain, forming an antiparallel sheet with the βB strand. E^{-5} faces a pocket formed by the βB strand, βC, and the βB–βC loop. (*E*) The canonical ligand-binding pocket of SNX27-PDZ-ESESKV. (*F*) The electropositive pocket (R56, R66, and R98) around the negatively charged E^{-5} is shown.

Remarkably, both IRK1*-$E^{-5}S^{-4}$ and IRK1*-$E^{-5}R^{-4}$ now exhibited binding to SNX27-PDZ (Fig. 3*B*). Conversely, GIRK3-$R^{-5}R^{-4}$ and GIRK3-$R^{-5}S^{-4}$ showed no binding to SNX27-PDZ (Fig. 3*B*). Taken together, these results indicate that the charge of the −5 position (Glu vs. Arg) is important for determining the binding to SNX27-PDZ. To investigate this further, we examined the effect of other substitutions in the −5 position (Fig. 3 *C* and *D*). These experiments revealed that SNX27-PDZ prefers acidic (Glu or Asp) or uncharged residues (Gln, Ala, or Trp) over basic (Lys or Arg) amino acids at the −5 position (Fig. 3 *C* and *D*). Interestingly, Trp substitution enhanced the relative SNX27-PDZ binding, suggesting the involvement of some interactions specific for the aromatic side chain. On the other hand, PSD95-PDZ1,2 favors basic and uncharged amino acids, but not acidic amino acids in the −5 position (Fig. 3*D*). Thus, with Arg in the −4 position, the charge of the −5 amino acid in the channel sequence can determine the binding specificity for PSD95 or SNX27.

We next examined whether changing the RR/ES sequence in the full-length channel would be sufficient to switch the functional association with SNX27 or PSD95. We examined the pattern of expression on the plasma membrane and submembrane regions with total internal reflection fluorescence (TIRF) microscopy (Fig. S4*A*) (24, 25). Similar to previous studies involving IRK channels (20), coexpression of PSD95-YFP with ^{CFP}IRK1* resulted in the formation of large clusters containing both proteins. In contrast, ^{CFP}IRK1*-$E^{-5}S^{-4}$ did not form clusters with PSD95-YFP (Fig. S4 *B* and *C*). On the other hand ^{CFP}GIRK3-$R^{-5}R^{-4}$ coexpressed with GIRK1, to promote plasma membrane targeting, now clustered with PSD95-YFP (Fig. S4 *D* and *E*).

We previously showed that SNX27b-YFP colocalizes with GIRK1/3 channels in submembrane early endosomal vesicles (Fig. 1 *B* and *C*) via the PX domain (6) (Fig. 4 *A* and *D*). Similarly, ^{CFP}IRK1*-$E^{-5}S^{-4}$, which binds SNX27-PDZ, showed clear areas of colocalization with SNX27b-YFP, in contrast to ^{CFP}IRK1* control (Fig. 4 *B* and *C*). Conversely, mutating the ES to RR in GIRK3 (^{CFP}GIRK3-$R^{-5}R^{-4}$) disrupted colocalization with SNX27b-YFP, consistent with a loss of SNX27-PDZ binding (Fig. 4 *C* and *D*).

To further investigate the functional effects of changes in PDZ selectivity, we measured the macroscopic currents in HEK293T cells transfected with channels and SNX27b (Fig. 5). We predicted that SNX27b would reduce IRK1*-$E^{-5}S^{-4}$ currents and would have little effect on GIRK3-$R^{-5}R^{-4}$ currents (6). Indeed, coexpressing SNX27b significantly reduced the Ba^{2+}-sensitive inwardly rectifying K^+ currents through IRK1*-$E^{-5}S^{-4}$ channels (Fig. 5 *A* and *B*). Interestingly, SNX27b expression enhanced IRK1* currents; this could involve other functional domains in SNX27. For example, SNX27 contains a Ras-associated domain that might interact with small GTPases (10), shown previously to alter trafficking of IRK1 channels (25). To study the G protein activation of GIRK3, we coexpressed GIRK3/GIRK1 and M_2 muscarinic receptors and then measured the carbachol-activated GIRK currents. In contrast to the significant reduction of carbachol-activated GIRK3/GIRK1 currents by SNX27b (Fig. 5*C*), the carbachol-activated currents for GIRK3-$R^{-5}R^{-4}$/GIRK1 were not significantly different from control (Fig. 5*D*). Thus, changing the charge of the amino acid in the −4/−5 positions (RR vs. ES) significantly alters the binding and functional association with SNX27 and PSD95.

We predicted that if changing the −4 and −5 positions were sufficient to switch the binding selectivity (Fig. 3), then analogous mutations in SNX27-PDZ might convert the PDZ-binding selectivity. We hypothesized that the positive charges formed by the βB–βC loop and part of the βB and βD strands could attract the acidic E^{-5} of GIRK3 while repelling the basic R^{-5} of IRK1 (Fig. 6*A*). Conversely, the surface charge map for the PSD95-PDZ2 structure where IRK1 tail was docked (26) shows a pattern of negative charges mapped to a smaller βB–βC loop, potentially interacting with the positively charged R^{-4} and R^{-5} of IRK1 (Fig. 6*A*). We altered the electrostatic properties of the SNX27-PDZ pocket by reversing the charge at R56 and R66 (Fig. 2*F*). The R56E mutation eliminated binding to GIRK3, whereas the R66E mutation introduced weak SNX27-PDZ binding to IRK1*; however, SNX27-PDZ-R66E retained binding

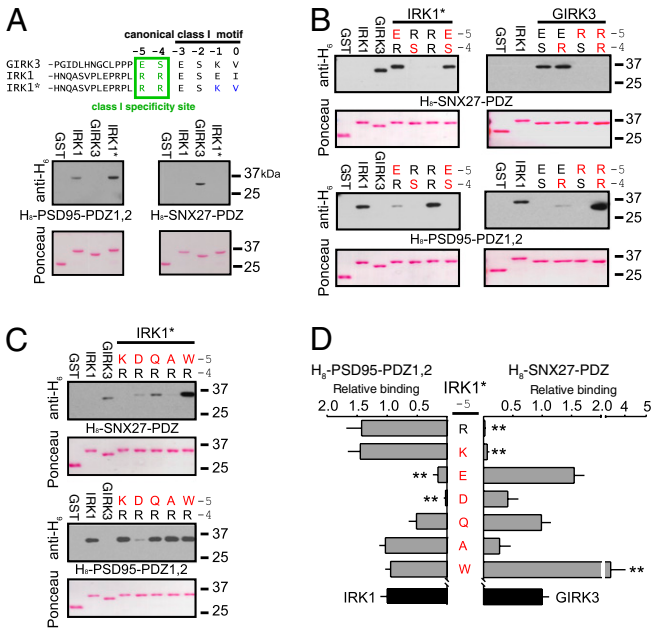

Fig. 3. Critical role for charge of the −5 residue in determining PDZ binding specificity for SNX27. (*A*) Amino acid sequence for GIRK3 and IRK1 C-terminal end (−3 to 0 residues) highlighted for the class I motif. An in vitro binding assay showed that converting $E^{-1}I^{0}$ to $K^{-1}V^{0}$ in IRK1 (IRK1*) does not create binding to SNX27-PDZ. (*B*) In vitro protein–protein binding assay with single or double mutations of the −5 and −4 positions in GIRK3 and IRK1*. (*C* and *D*) Effect of systematic substitutions at R^{-5} in IRK1* (Lys, Asp, Gln, Ala, or Trp) on binding to H_8-SNX27-PDZ or H_8-PSD95-PDZ1,2. (*D*) Bar graphs show quantification of binding to IRK1* mutants. SNX27-PDZ binding prefers ligands with acidic or neutral but not basic amino acids at the −5 position, whereas PSD95-PDZ1,2 prefers basic or neutral residues, but not acidic residues, at −5. Relative binding was normalized to GST-IRK1 and H_8-PSD95-PDZ1,2 or to GST-GIRK3 and H_8-SNX27-PDZ. Values are mean ± SEM. n = 3–5 experiments. $^{**}P < 0.05$ vs. WT channels.

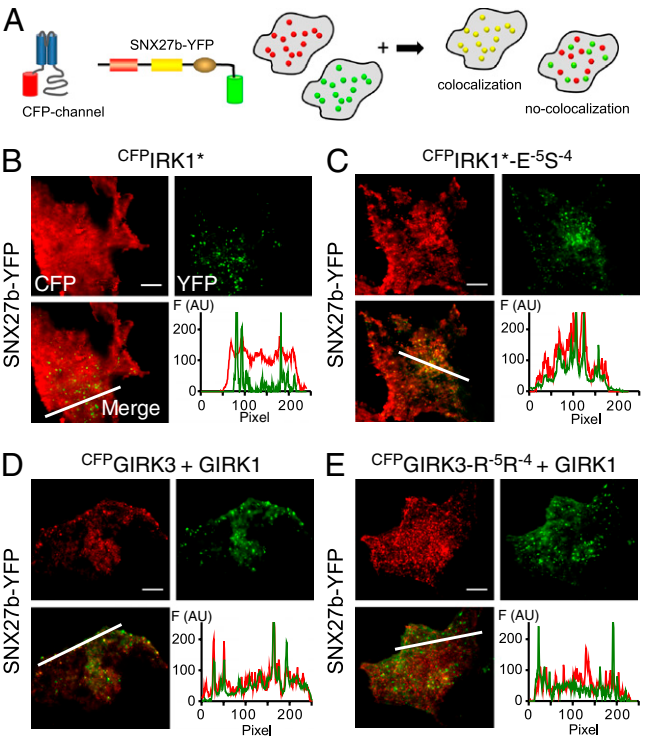

Fig. 4. Mutation of −5 and −4 residues reverses association and functional regulation of IRK1 and GIRK1/3 channels by SNX27b in COS7. (*A*) Cartoon illustrates the colocalization assay for CFP-tagged channel and YFP-tagged SNX27b using TIRF microscopy. If SNX27b and channel appear as overlapping puncta, then the two proteins colocalize. CFP is pseudo-colored red, and YFP is green. (*B*) SNX27b-YFP does not colocalize with WT ^{CFP}IRK1*. (*C*) In contrast, ^{CFP}IRK1*-$E^{-5}S^{-4}$ does colocalize with SNX27b. (*D*) Colocalization of ^{CFP}GIRK3 with SNX27b-YFP. (*E*) Colocalization is disrupted with the $R^{-5}R^{-4}$ mutation (^{CFP}GIRK3-$R^{-5}R^{-4}$). Graphs show fluorescence intensity for the line profile (white line in merged image). GIRK1 was coexpressed with ^{CFP}GIRK3 and ^{CFP}GIRK3-$R^{-5}R^{-4}$ to promote surface expression. (Scale bar: 10 μm.)

to GIRK3 (Fig. 6*B*). Combining R56E and R66E enhanced binding to IRK1* and, importantly, eliminated binding to GIRK3, indicating a preference for binding IRK1* over GIRK3 (Fig. 6*B*). Interestingly, SNX27-PDZ-R56E/R66E was able to bind IRK1*, but not WT IRK1. We speculated the hydrophobic pocket in SNX27-PDZ might be optimal for Val in the 0 position, and that I119 in SNX27-PDZ might sterically limit the size of amino acids in the 0 position. Indeed, the R56E/R66E/I119A triple mutation in SNX27-PDZ completely converted the binding selectivity from GIRK3 to WT IRK1 (Fig. 6*B*).

Discussion

Regulating surface expression of GIRK channels in the brain is important for controlling neuronal excitability (1). Here we show that SNX27a/b localizes in early endosomal compartments in hippocampal neurons and that expression of the methamphetamine-sensitive SNX27b isoform reduces $GABA_B$-GIRK currents. Previous studies suggested that reduced GIRK currents arise from the expression of fewer channels on the plasma membrane (6). Using a combination of biochemical, structural, and functional approaches, we determined the molecular mechanism by which SNX27 selects for GIRK3 and GIRK2c channels but not other ion channels containing a class I PDZ motif. Neurons contain an abundance of PDZ-containing proteins like SNX27 (19), and cellular signaling relies on specific interactions involving PDZ-containing proteins to create spatially and temporally limited functional complexes (27). Based on our findings, we propose an additional mechanism for PDZ-containing proteins to select appropriate target proteins and discuss the implication for neuronal signaling.

Previous strategies for refining the rules for classifying PDZ-containing proteins involved random peptide libraries, genome-wide scanning, and solving high-resolution structures. A screen of >100 PDZ domains with a C-terminal phage-display peptide library suggested that 16 distinct specificity classes exist, instead of the three classes identified previously (28). In contrast, protein microarray analysis of 157 PDZ domains suggested that PDZ domains cannot be placed into distinct classes, but rather exist along a continuum (29). These studies revealed important details regarding the complexities of PDZ binding but did not provide direct mechanistic insights into how proteins might fine-tune PDZ associations. Another approach has been to determine the structures of PDZ domains in complex with ligands. Generally, these structural studies revealed that the C-terminal peptide motif binds to a groove formed by the βB strand, αB helix, and carboxylate-binding GLGF loop of the PDZ protein (reviewed in ref. 18). These structural studies did not satisfactorily explain how channels with similar class I PDZ motifs bind to different PDZ domains.

Our experiments suggest that SNX27-PDZ–binding specificity is determined by two distinct structural regions, the classical binding site involving a hydrophobic groove near the 0 residue of the PDZ ligand and a second region containing a charged pocket formed around the −4 and −5 residues in the ligand (Fig. S5). In the classical site, the last four amino acids of the ligand (positions −3 to 0) interact with a binding cleft and the hydrophobic pocket formed by the αB helix, the βB strand, and the carboxylate-binding (i.e., GLGF) loop from the PDZ domain (23). Similar to previous studies (23, 30), we found that hydrophobic pocket plays an im-

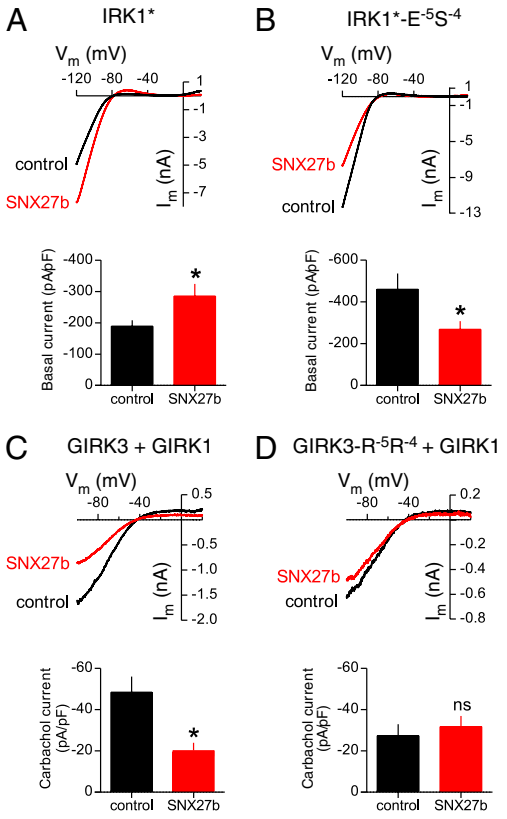

Fig. 5. Mutation of the −5 and −4 positions alters functional regulation of inwardly rectifying currents by SNX27b expressed in HEK293T cells. (*A* and *B*) Current-voltage plots shows examples of inwardly rectifying K^+ currents for IRK1* (*A*) and IRK1*-$E^{-5}S^{-4}$ (*B*) channels in the absence or presence of SNX27b (K_{out} = 5 mM). Bar graphs show mean values ± SEM (*n* = 11–14). SNX27b reduces the amplitude of Ba^{2+}-sensitive IRK1*-$E^{-5}S^{-4}$ currents while increasing the amplitude of IRK1* currents (see text). (*C* and *D*) Current-voltage plots show the effect of SNX27b on M_2 muscarinic receptor-activated (carbachol-induced) currents through GIRK1/GIRK3 (*C*) or GIRK1/GIRK3-$R^{-5}R^{-4}$ (*D*) channels (K_{out} = 20 mM). Bar graphs show mean induced currents ± SEM (*n* = 8–15) (Table S1). *$P < 0.05$, Student *t* test.

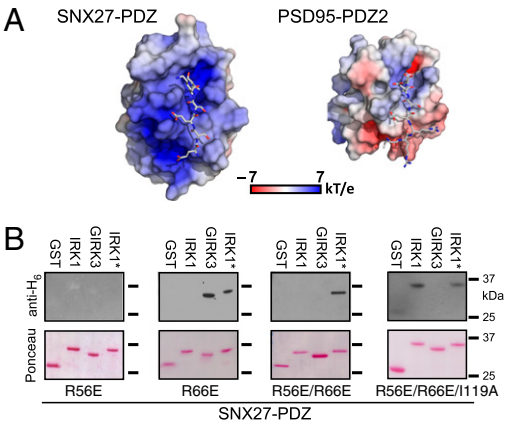

Fig. 6. Two sites involved in PDZ binding selectivity. A role for electrostatic potential of the βB–βC loop in determining SNX27 PDZ specificity. (A) Surface charge was mapped onto the molecular surface of SNX27-PDZ and PSD95-PDZ2 (26), with superimposed GIRK3 (-ESESKV) and IRK1 (-RRESEI) peptides, respectively. The negative E^{-5} of GIRK3 faces an electropositive groove between βB and the βB–βC loop of SNX27-PDZ. The positive R^{-5} and R^{-4} of IRK1 interact with negative charges near the αB helix of PSD95-PDZ2 (26). (*B*) SNX27 R56E eliminates binding, whereas an SNX27 R66E shows weak binding to IRK1* and GIRK3. SNX27 R56E/R66E creates selective binding to IRK1* and no detectable binding to GIRK3. Combining the I119A mutation in the 0 position with R56E/R66E converts SNX27-PDZ binding from GIRK3 to IRK1.

portant role in determining SNX27-PDZ binding; for example, a Val-to-Ile mutation in the C-terminal domain of GIRK3 eliminates binding to SNX27-PDZ (6), and similarly, a Val-to-Leu mutation in β1 adrenoreceptor switches the binding from SAP97-PDZ3 to NHERF-1 PDZ1 (30). Our structural analysis suggests that Ile is unfavorable in the 0 position, due to steric constraints.

In the second region, an electrostatic interaction occurs between a charged amino acid upstream of the canonical class I motif in GIRK3 (i.e., E^{-5}) and a structural pocket formed by charged residues in the βB–βC loop and the βB and βD strands of the PDZ domain. IRK1 is unable to bind to SNX27 because the positively charged R^{-5} is repulsed by the positive charges of R56 and R66 in the SNX27-PDZ domain. Consistent with this, two other known SNX27-interacting proteins, diacylglycerol kinase zeta (14) and cytohesin-associated scaffolding protein (31), contain a negatively charged −5 amino acid (Fig. S5). The 5-HT4a receptor or β2 adrenergic receptor, which also binds SNX27 (12, 13), contains a Ser or a Thr in the −5 position, respectively. Our mutational analysis of PDZ binding indicated that polar uncharged residues at the −5 position are permissive in the βB–βC binding pocket of SNX27 (Fig. 3 *C* and *D*). Previous studies have implicated residues upstream of the canonical motif in PDZ binding. Residue in the −6 position were found to be important for binding in a phage display study, but the role of the −5 position for SNX27-PDZ binding was considered less significant (28). Studies using a deletion analysis implicated a sequence upstream of the canonical binding motif but did not specify individual amino acids (20, 26). The possible involvement of the βB–βC region was suggested by previous structural analyses. A Trp at the −6 position was found to be important for binding to the βB–βC loop of ZO1-PDZ (32), and similarly, NMR studies have suggested that a −4 Trp interacts with the βB–βC loop from the Erbin PDZ domain (33). Collectively, these previous studies suggest that an interaction between upstream regions of the ligand and the βB–βC loop region may be important for binding.

We propose that variations in the βB–βC loop and charges surrounding this loop provide a mechanism for fine-tuning the binding of PDZ-containing proteins and establish the specificity needed for function (29, 34). For Kv1.4, CRIPT, and GluR6, the −5 residue is localized differently in the complexes with PSD95-PDZ1, suggesting that the proximity to the βB–βC loop might correlate with higher binding affinity (35). The βB–βC loop varies considerably among different PDZ domains (19) and is not essential for the binding for some PDZ proteins (36). Alternatively, the βB–βC loop in the protein tyrosine phosphatase BAS-like, PDZ2 domain folds back onto the protein backbone, providing structural support (37). In Shank-PDZ, the long βB–βC loop is involved in dimerization of two Shank-PDZ domains, but not in recognition of the −5 residue of the ligand (38). Thus, the βB–βC loop is an important variable component of the PDZ domain that might have evolved for specific functions for each PDZ domain. For some PDZ proteins, like SNX27, selective binding requires a proper fit of the ligand in both sites in the PDZ domain (Fig. S5).

Selectively inhibiting protein–protein interactions mediated by PDZ domains and neuronal proteins could be used to treat neuronal disorders (39). For example, small membrane-permeant peptides have been used to successfully antagonize interactions of NMDA receptors and PSD95 PDZ domains, providing protection of neurons from excitotoxicity and reduction of ischemic brain damage in rats (40). Current strategies are targeting only the canonical PDZ-binding groove, however (39). Improved selectivity and affinity might be achieved by engineering the −5 amino acid of the peptide to match the electrostatic properties of the βB–βC loop region in the PDZ domain. In the future, the selective dis-

ruption of SNX27–PDZ interactions might be used for treatment of drug addiction and memory disorders.

Materials and Methods

Detailed descriptions of the experimental procedures are provided in *SI Materials and Methods*. All animal experiments carried out in this study were reviewed and approved by the Salk Institute's Institutional Animal Care and Use Committee.

Fluorescent Immunohistochemistry. A polyclonal pan-SNX27 antibody was generated in rabbits immunized against peptide containing the first 18 residues of the N terminus of SNX27, followed by tyrosine (sequence: MADEDGEGIHPSTPHRNGY) following a standard protocol. Coronal sections of rat brain were stained with primary antibodies for SNX27 (rabbit), GFAP (mouse), NeuN (mouse), or MAP-2 (mouse), followed by incubation with appropriate fluorophore-conjugated secondary antibodies and imaging by laser confocal microscopy (Zeiss LSM5 PASCAL). Antibody specificity for SNX27 was assessed by inhibition with its cognate peptide (1 mg/mL; Fig. S1).

Molecular Biology. Full-length channels and SNX27b were cloned into pcDNA3.1(+), and PSD95 was cloned into a GWI-CMV vector. Carboxyl terminals of the channels were cloned into pGEX-2T, and PSD95-PDZ1,2 and SNX27-PDZ domains were cloned into a pHis8-3 vector. Point mutations were generated with the QuikChange XL Kit (Agilent) and confirmed by automated sequencing.

Cell Culture. Hippocampal neurons were isolated from 0- to 2-d-old rat pups and cultured in Neurobasal medium with B27 supplement (Invitrogen) (7). At DIV 4–5, cultures were infected with either SNX27b-YFP or GFP lentivirus. HEK293T and COS7 cells were maintained using standard protocols.

Protein-Binding Assay. In vitro protein-binding assays were carried out as described previously (6, 26).

Imaging. COS7 cells were transfected with 1 μg of CFP-tagged full-length channels and 1 μg of PSD95-YFP or SNX27b-YFP. After 48 h, cultures were imaged by TIRF microscopy (41).

Electrophysiology. HEK293T cells were transfected with 0.2 μg each of GIRK3, GIRK1, and M_2 receptor or 0.1 μg of IRK1* with or without 1 μg of SNX27b cDNA. After 48 h, currents were measured using a whole-cell patch clamp in 20 mM K_{out} (GIRK3/GIRK1 channels) or 5 mM K_{out} (IRK1* mutants). Native neuronal GIRK currents were measured at DIV 12–15 in 20 mM K_{out} with 100 μM APV, 10 μM CNQX, and 50 μM picrotoxin, as described previously (7).

Structural Studies. fWe solved crystal structures of SNX27-PDZ-ESESKV (PDB ID code 3QE1), SNX27-PDZ-GGESESKV (PDB ID code 3QDO) fusion constructs, and SNX27-PDZ complexed with free ESESKV peptide (PDB ID code 3QGL) using the molecular replacement method.

Statistical Analysis. Data are presented as mean ± SEM. Statistical differences were evaluated with the unpaired Student *t* test (two groups) or one-way ANOVA followed by Dunnett's post hoc test (three or more groups). A P value < 0.05 was considered statistically significant.

ACKNOWLEDGMENTS. We thank Joshua Tan, Steven M. Thomas, Jordan Sorokin, and Chris Childers for their help with the biochemistry; Natalie M. Taylor for the hippocampal neurons; Joan Vaughn for antibody production; Drs. Paul E. Sawchenko and Carlos Arias for help with the SNX27 antibody characterization; and Drs. Marc Montminy and Tony Hunter and members of the P.A.S. and S.C. laboratories for their insightful comments on the manuscript. Funding support was provided by the National Institute of Neurological Disorders and Stroke (Grant NS37682, to P.A.S.), National Alliance for Research on Schizophrenia and Depression (to P.A.S.), National Institute of General Medical Sciences (Grant GM521223, to S.C.), and National Institute on Drug Abuse (Grant DA019022, to P.A.S.).

1. Lüscher C, Slesinger PA (2010) Emerging roles for G protein-gated inwardly rectifying potassium (GIRK) channels in health and disease. *Nat Rev Neurosci* 11:301–315.
2. Reuveny E, et al. (1994) Activation of the cloned muscarinic potassium channel by G protein βγ subunits. *Nature* 370:143–146.
3. Wickman KD, et al. (1994) Recombinant G-protein βγ-subunits activate the muscarinic-gated atrial potassium channel. *Nature* 368:255–257.
4. Chung HJ, Qian X, Ehlers M, Jan YN, Jan LY (2009) Neuronal activity regulates phosphorylation-dependent surface delivery of G protein-activated inwardly rectifying potassium channels. *Proc Natl Acad Sci USA* 106:629–634.
5. Huang CS, et al. (2005) Common molecular pathways mediate long-term potentiation of synaptic excitation and slow synaptic inhibition. *Cell* 123:105–118.
6. Lunn ML, et al. (2007) A unique sorting nexin regulates trafficking of potassium channels via a PDZ domain interaction. *Nat Neurosci* 10:1249–1259.
7. Nassirpour R, et al. (2010) Morphine- and CaMKII-dependent enhancement of GIRK channel signaling in hippocampal neurons. *J Neurosci* 30:13419–13430.
8. Ma D, et al. (2002) Diverse trafficking patterns due to multiple traffic motifs in G protein-activated inwardly rectifying potassium channels from brain and heart. *Neuron* 33:715–729.
9. Mirshahi T, Logothetis DE (2004) Molecular determinants responsible for differential cellular distribution of G protein-gated inwardly rectifying K^+ channels. *J Biol Chem* 279:11890–11897.
10. Cullen PJ (2008) Endosomal sorting and signalling: An emerging role for sorting nexins. *Nat Rev Mol Cell Biol* 9:574–582.
11. Munton RP, et al. (2007) Qualitative and quantitative analyses of protein phosphorylation in naive and stimulated mouse synaptosomal preparations. *Mol Cell Proteomics* 6:283–293.
12. Joubert L, et al. (2004) New sorting nexin (SNX27) and NHERF specifically interact with the 5-HT4a receptor splice variant: Roles in receptor targeting. *J Cell Sci* 117:5367–5379.
13. Lauffer BE, et al. (2010) SNX27 mediates PDZ-directed sorting from endosomes to the plasma membrane. *J Cell Biol* 190:565–574.
14. Rincón E, et al. (2007) Proteomics identification of sorting nexin 27 as a diacylglycerol kinase zeta-associated protein: New diacylglycerol kinase roles in endocytic recycling. *Mol Cell Proteomics* 6:1073–1087.
15. Fujiyama K, Kajii Y, Hiraoka S, Nishikawa T (2003) Differential regulation by stimulants of neocortical expression of *mrt1*, *arc*, and *homer1a* mRNA in the rats treated with repeated methamphetamine. *Synapse* 49:143–149.
16. Kajii Y, et al. (2003) A developmentally regulated and psychostimulant-inducible novel rat gene *mrt1* encoding PDZ-PX proteins isolated in the neocortex. *Mol Psychiatry* 8:434–444.
17. Songyang Z, et al. (1997) Recognition of unique carboxyl-terminal motifs by distinct PDZ domains. *Science* 275:73–77.
18. Hung AY, Sheng M (2002) PDZ domains: Structural modules for protein complex assembly. *J Biol Chem* 277:5699–5702.
19. Kim E, Sheng M (2004) PDZ domain proteins of synapses. *Nat Rev Neurosci* 5:771–781.
20. Nehring RB, et al. (2000) Neuronal inwardly rectifying K(+) channels differentially couple to PDZ proteins of the PSD-95/SAP90 family. *J Neurosci* 20:156–162.
21. Leonoudakis D, et al. (2004) Protein trafficking and anchoring complexes revealed by proteomic analysis of inward rectifier potassium channel (Kir2.x)-associated proteins. *J Biol Chem* 279:22331–22346.
22. Inanobe A, et al. (1999) Characterization of G-protein-gated K^+ channels composed of Kir3.2 subunits in dopaminergic neurons of the substantia nigra. *J Neurosci* 19:1006–1017.
23. Doyle DA, et al. (1996) Crystal structures of a complexed and peptide-free membrane protein-binding domain: Molecular basis of peptide recognition by PDZ. *Cell* 85:1067–1076.
24. Riven I, Iwanir S, Reuveny E (2006) GIRK channel activation involves a local rearrangement of a preformed G protein channel complex. *Neuron* 51:561–573.
25. Boyer SB, Slesinger PA, Jones SV (2009) Regulation of Kir2.1 channels by the Rho-GTPase, Rac1. *J Cell Physiol* 218:385–393.
26. Pegan S, et al. (2007) NMR studies of interactions between C-terminal tail of Kir2.1 channel and PDZ1,2 domains of PSD95. *Biochemistry* 46:5315–5322.
27. Long JF, et al. (2003) Supramodular structure and synergistic target binding of the N-terminal tandem PDZ domains of PSD-95. *J Mol Biol* 327:203–214.
28. Tonikian R, et al. (2008) A specificity map for the PDZ domain family. *PLoS Biol* 6:e239.
29. Stiffler MA, et al. (2007) PDZ domain binding selectivity is optimized across the mouse proteome. *Science* 317:364–369.
30. He J, et al. (2006) Proteomic analysis of beta1-adrenergic receptor interactions with PDZ scaffold proteins. *J Biol Chem* 281:2820–2827.
31. MacNeil AJ, Mansour M, Pohajdak B (2007) Sorting nexin 27 interacts with the Cytohesin-associated scaffolding protein (CASP) in lymphocytes. *Biochem Biophys Res Commun* 359:848–853.
32. Appleton BA, et al. (2006) Comparative structural analysis of the Erbin PDZ domain and the first PDZ domain of ZO-1: Insights into determinants of PDZ domain specificity. *J Biol Chem* 281:22312–22320.
33. Skelton NJ, et al. (2003) Origins of PDZ domain ligand specificity: Structure determination and mutagenesis of the Erbin PDZ domain. *J Biol Chem* 278:7645–7654.
34. Chen JR, Chang BH, Allen JE, Stiffler MA, MacBeath G (2008) Predicting PDZ domain–peptide interactions from primary sequences. *Nat Biotechnol* 26:1041–1045.
35. Piserchio A, Spaller M, Mierke DF (2006) Targeting the PDZ domains of molecular scaffolds of transmembrane ion channels. *AAPS J* 8:E396–E401.
36. von Ossowski I, et al. (2006) Crystal structure of the second PDZ domain of SAP97 in complex with a GluR-A C-terminal peptide. *FEBS J* 273:5219–5229.
37. Walma T, et al. (2002) Structure, dynamics and binding characteristics of the second PDZ domain of PTP-BL. *J Mol Biol* 316:1101–1110.
38. Birrane G, Chung J, Ladias JA (2003) Novel mode of ligand recognition by the Erbin PDZ domain. *J Biol Chem* 278:1399–1402.
39. Blazer LL, Neubig RR (2009) Small molecule protein–protein interaction inhibitors as CNS therapeutic agents: Current progress and future hurdles. *Neuropsychopharmacology* 34: 126–141.
40. Aarts M, et al. (2002) Treatment of ischemic brain damage by perturbing NMDA receptor–PSD-95 protein interactions. *Science* 298:846–850.
41. Fowler CE, Aryal P, Suen KF, Slesinger PA (2007) Evidence for association of GABA(B) receptors with Kir3 channels and regulators of G protein signalling (RGS4) proteins. *J Physiol* 580:51–65.